Cell tracking and detection of molecular expression in live cells using lipid-enclosed CdSe quantum dots as contrast agents for epi-third harmonic generation microscopy

Chieh-Feng Chang,[1] Chao-Yu Chen,[2] Fu-Hsiung Chang,[2]* Shih-Peng Tai,[1] Cheng-Ying Chen,[1] Che-Hang Yu,[1] Yi-Bing Tseng,[1] Tsung-Han Tsai,[1] I-Shuo Liu,[3] Wei-Fang Su,[3] and Chi-Kuang Sun[1,4]*

[1]*Department of Electrical Engineering and Graduate Institute of Photonics and Optoelectronics, National Taiwan University, Taipei 10617, Taiwan*
[2]*Graduate Institute of Biochemistry and Molecular Biology, National Taiwan University, Taipei, Taiwan*
[3]*Institute of Material Sciences, College of Engineering, National Taiwan University, Taipei, Taiwan*
[4]*Research Center for Applied Sciences, Academia Sinica, Taipei 10617, Taiwan*
[*]*Corresponding authors: sun@cc.ee.ntu.edu.tw; fhchang@ntu.edu.tw*

Abstract: We demonstrated that lipid-enclosed CdSe quantum dots (LEQDs) can function as versatile contrast agents in epi-detection third harmonic generation (THG) microscopy for biological applications *in vivo*. With epi-THG intensities 20 times stronger than corresponding fluorescence intensities from the same LEQDs under the same conditions of energy absorption, such high brightness LEQDs were proved for the abilities of cell tracking and detection of specific molecular expression in live cancer cells. Using nude mice as an animal model, the distribution of LEQD-loaded tumor cells deep in subcutaneous tissues were imaged with high THG contrast. This is the first demonstration that THG contrast can be manipulated *in vivo* with nanoparticles. By linking LEQDs with anti-Her2 antibodies, the expression of Her2/neu receptors in live breast cancer cells could also be easily detected through THG. Compared with fluorescence modalities, the THG modality also provides the advantage of no photobleaching and photoblinking effects. Combined with a high penetration 1230 nm laser, these novel features make LEQDs excellent THG contrast agents for *in vivo* deep-tissue imaging in the future.

OCIS codes: (180.6900) Three-dimensional microscopy; (180.5810) Scanning microscopy; (190.4160) Multiharmonic generation.

References and links

1. D. Yelin and Y. Silberberg, "Laser scanning third-harmonic-generation microscopy in biology," Opt. Express **5**, 169-175 (1999), http://www.opticsinfobase.org/abstract.cfm?URI=oe-5-8-169.
2. S.-W. Chu, S.-Y. Chen, T.-H. Tsai, T.-M. Liu, C.-Y. Lin, H.-J. Tsai, and C.-K. Sun, "*In vivo* developmental biology study using noninvasive multi-harmonic generation microscopy," Opt. Express **11**, 3093-3099 (2003), http://www.opticsinfobase.org/abstract.cfm?URI=oe-11-23-3093.
3. C.-K. Sun, S.-W. Chu, S.-Y. Chen, T.-H. Tsai, T.-M. Liu, C.-Y. Lin, and H.-J. Tsai, "Higher harmonic generation microscopy for developmental biology," J. Struct. Biol. **147**, 19-30 (2004).
4. D. Debarre, W. Supatto, E. Farge, B. Moulia, M. C. Schanne-Klein, and E. Beaurepaire, "Velocimetric third-harmonic generation microscopy: micrometer-scale quantification of morphogenetic movements in unstained embryos," Opt. Lett. **29**, 2881-2883 (2004).
5. W. Supatto, D. Debarre, B. Moulia, E. Brouzes, J. L. Martin, E. Farge, and E. Beaurepaire, "*In vivo* modulation of morphogenetic movements in Drosophila embryos with femtosecond laser pulses," Proc. Nat. Acad. Sci. U.S.A. **102**, 1047-1052 (2005).
6. D. Debarre, W. Supatto, A. M. Pena, A. Fabre, T. Tordjmann, L. Combettes, M. C. Schanne-Klein, and E. Beaurepaire, "Imaging lipid bodies in cells and tissues using third-harmonic generation microscopy," Nat. Methods **3**, 47-53 (2006).

#93051 - $15.00 USD Received 22 Feb 2008; revised 26 May 2008; accepted 27 May 2008; published 13 Jun 2008

7. T.-H. Tsai, C.-Y. Lin, H.-J. Tsai, S.-Y. Chen, S.-P. Tai, K.-H. Lin, and C.-K. Sun, "Biomolecular imaging based on far-red fluorescent protein with a high two-photon excitation action cross section," Opt. Lett. **31**, 930-932 (2006).
8. S.-P. Tai, W.-J. Lee, D.-B. Shieh, P.-C. Wu, H.-Y. Huang, C.-H. Yu, and C.-K. Sun, "*In vivo* optical biopsy of hamster oral cavity with epi-third-harmonic-generation microscopy," Opt. Express **14**, 6178-6187 (2006), http://www.opticsinfobase.org/abstract.cfm?URI=oe-14-13-6178.
9. S.-Y. Chen, C.-S. Hsieh, S.-W. Chu, C.-Y. Lin, C.-Y. Ko, Y.-C. Chen, H.-J. Tsai, C.-H. Hu, and C.-K. Sun, "Noninvasive harmonics optical microscopy for long-term observation of embryonic nervous system development *in vivo*," J. Biomed. Opt. **11**, 054022 (2006).
10. C.-H. Yu, S.-P. Tai, C.-T. Kung, I.-J. Wang, H.-C. Yu, H.-J. Huang, W.-J. Lee, Y.-F. Chan, and C.-K. Sun, "*In vivo* and *ex vivo* imaging of intra-tissue elastic fibers using third-harmonic-generation microscopy," Opt. Express **15**, 11167-11177 (2007), http://www.opticsinfobase.org/abstract.cfm?URI=oe-15-18-11167.
11. E. J. Gualda, G. Filippidis, G. Voglis, M. Mari, C. Fotakis, and N. Tavernarakis, "*In vivo* imaging of cellular structures in Caenorhabditis elegans by combined TPEF, SHG and THG microscopy," J. Microsc. **229**, 141-150 (2008).
12. V. Barzda, C. Greenhalgh, J. Aus der Au, S. Elmore, J. van Beek, and J. Squier, "Visualization of mitochondria in cardiomyocytes by simultaneous harmonic generation and fluorescence microscopy," Opt. Express **13**, 8263-8276 (2005), http://www.opticsinfobase.org/abstract.cfm?URI=oe-13-20-8263.
13. S.-W. Chu, I.-H. Chen, T.-M. Liu, C.-K. Sun, S.-P. Lee, B.-L. Lin, P.-C. Cheng, M.-X. Kuo, D.-J. Lin, and H.-L. Liu, "Nonlinear bio-photonic crystal effects revealed with multimodal nonlinear microscopy," J. Microsc. **208**, 190-200 (2002).
14. C.-K. Sun, C.-C. Chen, S.-W. Chu, T.-H. Tsai, Y.-C. Chen, and B.-L. Lin, "Multiharmonic-generation biopsy of skin," Opt. Lett. **28**, 2488-2490 (2003).
15. S.-P. Tai, T.-H. Tsai, W.-J. Lee, D.-B. Shieh, Y.-H. Liao, H.-Y. Huang, K. Zhang, H.-L. Liu, and C.-K. Sun, "Optical biopsy of fixed human skin with backward-collected optical harmonics signals," Opt. Express **13**, 8231-8242 (2005), http://www.opticsinfobase.org/abstract.cfm?URI=oe-13-20-8231.
16. R. R. Anderson, and J. A. Parrish, "The Optics of Human Skin," J. Invest. Dermatol. **77**, 13-19 (1981).
17. C.-K. Sun, *Series in Advances in Biochemical Engineering/Biotechnology, Special Volume 95: Microscopy Techniques* (Springer-Verlag, Berlin, 2005), Chap. "Higher harmonic generation microscopy."
18. S.-W. Chu, S.-P. Tai, C.-L. Ho, C.-H. Lin, and C.-K. Sun, "High-resolution simultaneous three-photon fluorescence and third-harmonic-generation microscopy," Microsc. Res. Tech **66**, 193-197 (2005).
19. G. O. Clay, A. C. Millard, C. B. Schaffer, J. Aus-der-Au, P. S. Tsai, J. A. Squier, and D. Kleinfeld, "Spectroscopy of third-harmonic generation: evidence for resonances in model compounds and ligated hemoglobin," J. Opt. Soc. Am. B: Opt. Phys. **23**, 932-950 (2006).
20. R. D. Schaller, J. C. Johnson, and R. J. Saykally, "Nonlinear Chemical Imaging Microscopy: Near-Field Third Harmonic Generation Imaging of Human Red Blood Cells," Anal. Chem **72**, 5361-5364 (2000).
21. H. Kano and S. Kawata, "Two-photon-excited fluorescence enhanced by a surface plasmon," Opt. Lett. **21**, 1848-1850 (1996).
22. K. Kneipp, H. Kneipp, I. Itzkan, R. R. Dasari, and M. S. Feld, "Ultrasensitive chemical analysis by Raman spectroscopy," Chem. Rev. **99**, 2957-2976 (1999).
23. B. Lamprecht, J. R. Krenn, A. Leitner, and F. R. Aussenegg, "Resonant and Off-Resonant Light-Driven Plasmons in Metal Nanoparticles Studied by Femtosecond-Resolution Third-Harmonic Generation," Phys. Rev. Lett. **83**, 4421-4424 (1999).
24. T.-M. Liu, S.-P. Tai, C.-H. Yu, Y.-C. Wen, S.-W. Chu, L.-J. Chen, M. R. Prasad, K.-J. Lin, and C.-K. Sun, "Measuring plasmon-resonance enhanced third-harmonic $\chi^{(3)}$ of Ag nanoparticles," Appl. Phys. Lett. **89**, 043122 (2006).
25. S. Nie and S. R. Emory, "Probing Single Molecules and Single Nanoparticles by Surface-Enhanced Raman Scattering," Science **275**, 1102 (1997).
26. A. Podlipensky, J. Lange, G. Seifert, H. Graener, and I. Cravetchi, "Second-harmonic generation from ellipsoidal silver nanoparticles embedded in silica glass," Opt. Lett. **28**, 716-718 (2003).
27. S.-P. Tai, Y. Wu, D.-B. Shieh, L.-J. Chen, K.-J. Lin, C.-H. Yu, S.-W. Chu, C.-H. Chang, X.-Y. Shi, Y.-C. Wen, K.-H. Lin, T.-M. Liu, and C.-K. Sun, "Molecular Imaging of Cancer Cells Using Plasmon-Resonant-Enhanced Third-Harmonic-Generation in Silver Nanoparticles," Adv. Mater. **19**, 4520-4523 (2007).
28. D. Yelin, D. Oron, S. Thiberge, E. Moses, and Y. Silberberg, "Multiphoton plasmon-resonance microscopy," Opt. Express **11**, 1385-1391 (2003), http://www.opticsinfobase.org/abstract.cfm?URI=oe-11-12-1385.
29. M. Lippitz, M. A. van Dijk, and M. Orrit, "Third-harmonic generation from single gold nanoparticles," Nano Lett. **5**, 799–802 (2005).
30. X. Michalet, F. F. Pinaud, L. A. Bentolila, J. M. Tsay, S. Doose, J. J. Li, G. Sundaresan, A. M. Wu, S. S. Gambhir, and S. Weiss, "Quantum dots for live cells, *in vivo* imaging, and diagnostics," Science **307**, 538-544 (2005).
31. E. B. Voura, J. K. Jaiswal, H. Mattoussi, and S. M. Simon, "Tracking metastatic tumor cell extravasation with quantum dot nanocrystals and fluorescence emission-scanning microscopy," Nat. Med. **10**, 993-998 (2004).

#93051 - $15.00 USD Received 22 Feb 2008; revised 26 May 2008; accepted 27 May 2008; published 13 Jun 2008

32. A. K. Dharmadhikari, N. Kumbhojkar, J. A. Dharmadhikari, S. Mahamuni, and R. C. Aiyer, "Studies on third-harmonic generation in chemically grown ZnS quantum dots," J. Phys.: Condens. Matter **11**, 1363-1368 (1999).
33. D. Mohanta, G. A. Ahmed, A. Choudhury, F. Singh, D. K. Avasthi, G. Boyer, and G. A. Stanciu, "Scanning probe microscopy, luminescence and third harmonic generation studies of elongated CdS:Mn nanostructures developed by energetic oxygen-ion-impact," Eur. Phys. J.: Appl. Phys. **35**, 29-36 (2006).
34. S. Sauvage, P. Boucaud, F. Glotin, R. Prazeres, J. M. Ortega, A. Lemaitre, J. M. Gerard, and V. Thierry-Mieg, "Third-harmonic generation in InAs/GaAs self-assembled quantum dots," Phys. Rev. B **59**, 9830-9833 (1999).
35. C.-H. Yu, S.-P. Tai, C.-T. Kung, W.-J. Lee, Y.-F. Chan, H.-L. Liu, J.-Y. Lyu, and C.-K. Sun, "Molecular third-harmonic-generation microscopy through resonance enhancement with absorbing dye," Opt. Lett. **33**, 387-389 (2008).
36. M. A. Hines and P. Guyot-Sionnest, "Synthesis and characterization of strongly luminescing ZnS-Capped CdSe nanocrystals," J. Phys. Chem. **100**, 468-471 (1996).
37. C. B. Murray, D. J. Norris, and M. G. Bawendi, "Synthesis and characterization of nearly monodisperse CdE (E= sulfur, selenium, tellurium) semiconductor nanocrystallites," J. Am. Chem. Soc. **115**, 8706-8715 (1993).
38. C.-Y. Chen, S. R. Roffler, I.-S. Liu, C.-C. Liu, W.-F. Su, and F.-H. Chang are preparing a manuscript to be called "Facile and efficient assembly of antibody-tagged quantum dots for membrane receptor targeting."
39. B. Dubertret, P. Skourides, D. J. Norris, V. Noireaux, A. H. Brivanlou, and A. Libchaber, "*In Vivo* Imaging of Quantum Dots Encapsulated in Phospholipid Micelles," Science **298**, 1759 (2002).
40. J. X. Cheng and X. S. Xie, "Green's function formulation for third-harmonic generation microscopy," J. Opt. Soc. Am. B: Opt. Phys. **19**, 1604-1610 (2002).
41. M. J. Weber, *Handbook of Optical Materials* (CRC Press, 2003).
42. J. M. Schins, T. Schrama, J. Squier, G. J. Brakenhoff, and M. Muller, "Determination of material properties by use of third-harmonic generation microscopy," J. Opt. Soc. Am. B: Opt. Phys. **19**, 1627-1634 (2002).
43. J. T. Seo, S. M. Ma, Q. Yang, L. Creekmore, R. Battle, H. Brown, A. Jackson, T. Skyles, B. Tabibi, and W. Yu, "Large Resonant Third-order Optical Nonlinearity of CdSe Nanocrystal Quantum Dots," J. Phys.: Conf. Ser. **38**, 91-94 (2006).
44. D. Debarre, N. Olivier, and E. Beaurepaire, "Signal epidetection in third-harmonic generation microscopy of turbid media," Opt. Express **15**, 8913-8924 (2007), http://www.opticsinfobase.org/abstract.cfm?URI=oe-15-14-8913.
45. G. Veres, S. Matsumoto, Y. Nabekawa, and K. Midorikawa, "Enhancement of third-harmonic generation in absorbing media," Appl. Phys. Lett. **81**, 3714-3716 (2002).
46. C. J. Murphy, "Optical sensing with quantum dots," Anal. Chem. **74**, 520A-526A (2002).
47. M. Campiglio, A. Locatelli, C. Olgiati, N. Normanno, G. Somenzi, L. Vigano, M. Fumagalli, S. Menard, and L. Gianni, "Inhibition of proliferation and induction of apoptosis in breast cancer cells by the epidermal growth factor receptor(EGFR) tyrosine kinase inhibitor ZD 1839('Iressa') is independent of EGFR expression level," J. Cell. Physiol. **198**, 259-268 (2004).
48. T. Faltus, J. Yuan, B. Zimmer, A. Kramer, S. Loibl, M. Kaufmann, and K. Strebhardt, "Silencing of the HER2/neu gene by siRNA inhibits proliferation and induces apoptosis in HER2/neu-overexpressing breast cancer cells," Neoplasia **6**, 786-795 (2004).
49. W. L. Xia, J. Bisi, J. Strum, L. H. Liu, K. Carrick, K. M. Graham, A. L. Treece, M. A. Hardwicke, M. Dush, Q. Y. Liao, R. E. Westlund, S. M. Zhao, S. Bacus, and N. L. Spector, "Regulation of survivin by ErbB2 signaling: Therapeutic implications for ErbB2-overexpressing breast cancers," Cancer Res. **66**, 1640-1647 (2006).
50. D. R. Emlet, R. Schwartz, K. A. Brown, A. A. Pollice, C. A. Smith, and S. E. Shackney, "HER2 expression as a potential marker for response to therapy targeted to the EGFR," Br. J. Cancer **94**, 1144-1153 (2006).
51. K. I. Pritchard, L. E. Shepherd, F. P. O'Malley, I. L. Andrulis, D. S. Tu, V. H. Bramwell, and M. N. Levine, "HER2 and responsiveness of breast cancer to adjuvant chemotherapy," N. Engl. J. Med. **354**, 2103-2111 (2006).
52. O. Thuerigen, A. Schneeweiss, G. Toedt, P. Warnat, M. Halm, H. Kramer, B. Brors, C. Rudlowski, A. Benner, F. Schuetz, B. Tews, R. Eils, H. P. Sinn, C. Sohn, and P. Lichter, "Gene expression signature predicting pathologic complete response with gemcitabine, epirubicin, and docetaxel in primary breast cancer," J. Clin. Oncol. **24**, 1839-1845 (2006).
53. G. L. Plosker and S. J. Keam, "Trastuzumab - A review of its use in the management of HER2-positive metastatic and early-stage breast cancer," Drugs **66**, 449-475 (2006).
54. S. S. Bacus, K. Kiguchi, D. Chin, C. R. King, and E. Huberman, "Differentiation of Cultured Human Breast Cancer Cells (AU-565 and MCF-7) Associated with Loss of Cell Surface HER-2/neu Antigen," Mol. Carcinog. **3**, 350-362 (1990).

#93051 - $15.00 USD Received 22 Feb 2008; revised 26 May 2008; accepted 27 May 2008; published 13 Jun 2008

1. Introduction

In recent years, third harmonic generation (THG) microscopy has emerged as an important least-invasive imaging modality in biological research, especially in intravital and *in vivo* applications [1-11]. The advantages of THG microscopy for biological imaging are manifold, including its intrinsic optical sectioning capability due to the high-order nonlinearity nature and minimized energy release due to the virtual-state-transition characteristic [6, 12-15]. Combined with an excitation source at 1230 nm, which is situated in the optical penetration window of most biological tissues [16], THG microscopy can provide an enhanced observation depth and much reduced photodamage than other microscopy techniques using a shorter excitation wavelength, such as confocal or two-photon fluorescence microscopy [3]. These combined features make THG microscopy particularly favorable because minimum invasion is achieved and cell viability can be greatly improved [3, 9]. Other benefits of THG versus fluorescence-based technologies include the absence of photobleaching and photoblinking effects [17], making long-term observation much more feasible. However the endogenous contrast of THG is limited in animals, dominated by cell membranes [2, 9], lipid bodies [6], mitochondria [12, 18], hemoglobin [19, 20] and elastin fibrils [10]. As a result, developing exogenous THG contrast agents to manipulate the contrast mechanism or to trace the functions of specific molecules should thus be highly desirable. Noble metal nanoparticles, such as those of gold or silver, have been shown to enhance various types of nonlinear optical signals through surface plasmon resonances (SPR) [21-28]. In a previous study, we demonstrated molecule-specific THG microscopy using silver nanoparticles as contrast agents to image the expression of Her2/neu receptors in fixed mouse bladder cells [27]. To use metal nanoparticles as contrast agents, however, would require matching the THG or the laser wavelength to the SPR wavelength; this fixes the size of metal nanoparticles and therefore limits their THG efficiency [29]. As a result, we would like to develop efficient THG contrast agents that are bright and functional in all excitation wavelengths. Recently, quantum dots (QDs) have been widely used as fluorescence tags for labeling cells and for other *in vivo* studies due to several advantages, including high quantum efficiency, narrow emission spectra, and insensitivity to excitation laser wavelength [30, 31]. These characteristics make QDs ideal for multicolor labeling simultaneously excited by one laser. THG from QDs were also reported in recent studies [32-34], thus putting them on the list of possible contrast agents in THG microscopy for biomolecular imaging.

In this paper, we developed lipid-enclosed quantum dots (LEQDs) that are functional under different excitation sources to act as efficient THG contrast agents for contrast manipulation and for molecular imaging. Due to coherent effects, the epi-THG intensity from an LEQD was found to nonlinearly increase with the particle size and would reach saturation when the particle diameter exceeded 100 nm, beginning from which destructive interference from different parts of a large nanoparticle would occur. Enhanced by three-photon resonance, the detected epi-THG intensities of ~130 nm LEQDs were found to be 20 times stronger than the corresponding fluorescence intensities from the same LEQDs under the same conditions of energy absorption. We then demonstrated that such high-THG-brightness LEQDs could be used to label live cells for *in vivo* cell tracking and for detection of specific molecular expression. Using nude mice as an animal model, CT-26 tumor cells loaded with LEQD could be clearly imaged *in vivo* by epi-THG microscopy deep in subcutaneous tissues. We also performed experiments on cultured human breast cancer cells and proved that the abilities of high-brightness LEQDs could be further extended to the detection of specific molecular expression. By linking LEQDs with anti-Her2 antibodies, AU565 cells with high Her2/neu receptor expression on cell surfaces could be selectively identified from other cell lines with low expression. These experiments indicated that through the THG mechanism LEQDs can provide even brighter signals than fluorescence under the same condition of energy deposition, which enables higher cell viability and a much improved penetration depth. As a further step from the manipulation of THG contrast we previously reported in fixed cells, *ex vivo*, or using acetic acid [10, 27, 35], these results demonstrated for the first time that THG contrast can be

#93051 - $15.00 USD Received 22 Feb 2008; revised 26 May 2008; accepted 27 May 2008; published 13 Jun 2008

manipulated *in vivo* using nanoparticles in live animals. Combined with the high-penetration and high-viability capabilities of the excitation laser [3], these unique features make LEQDs excellent THG contrast agents for future microscopy applications *in vivo*, especially when deep-tissue biomolecular imaging or contrast manipulation is required.

2. Materials and methods

2.1 Synthesis of lipid-enclosed CdSe quantum dots

The CdSe QDs were synthesized following the standard procedure using trioctylphosphine oxide (TOPO) as the stabilizing agent [36, 37]. They had a narrow size distribution (~5 nm in diameter), good photoluminescence properties (580 nm emission maximum), and remained stable for at least 3 months in organic solutions. To further apply the lipid coating, CdSe QDs and lipids were mixed in chloroform, desiccated by evaporation of chloroform, and re-suspended in 5% dextrose solution by sonication to form LEQDs. Two kinds of lipid combinations were used for different applications. The composition for neutral LEQDs in this study included 1,2-Dipalmitoyl-*sn*-Glycero-3-phosphocholine (DPPC) and cholesterol that were mixed in a 1:1 molar ratio and added with 1% of 1,2-Dioleoyl-*sn*-Glycero-3-phosphoethanolamine-N-[methoxy(poly(ethyleneglycol)-2000)] (DOPE-PEG) and 0.1% of 1,2-Dioleoyl-*sn*-Glycero-3-phosphoethanolamine-n-biotin (DOPE-biotin) (Avanti Polar Lipids, AL, USA). To improve particle solubility and cell uptake, the lipid ingredients 3-β-[N-(2-guanidinoethyl)carbamoyl]-cholesterol (GEC-Chol) and cholesterol (in a 1:1 molar ratio) were used in the formulation of cationic LEQDs. The absorption and fluorescence spectra of these aqueous LEQDs were determined by a photoluminometer (Perkin Elmer LS55, USA) and a UV-visible spectrometer (Perkin Elmer 35, USA). No significant difference in photoluminescence properties was found between LEQDs—whether freshly prepared or stored in aqueous solutions—and TOPO-stabilized QD in organic solutions up to 2 months [38]. Figure 1(a) shows the absorption and emission spectra of the synthesized CdSe QDs. The emission peak was ~580 nm and the absorption increased rapidly in the UV range, including the THG wavelength of 410 nm investigated in this paper. The diameters of LEQDs were measured by a dynamic light scattering particle analyzer (Malvern Nano-ZS90, UK). The LEQDs were also imaged with a transmission electron microscope (TEM), and Fig. 1(b) shows a TEM graph of ~100 nm CdSe LEQDs. Since negative staining was not applied, the dried, contracted lipid regions could not be seen and CdSe QDs appeared as clusters. More than ten CdSe QDs were observed inside each lipid sphere. The procedure of enclosing small QDs with lipids provides the following benefits. First, the particle size can be increased to more than 100 nm for high epi-THG brightness, and pure quantum dots this large could be difficult to synthesize in aqueous form. Second, while metal nanoparticles can also be made larger to increase the THG efficiency, the SPR wavelength would shift and render them useless for the same laser. Third, we can choose different lipids to synthesize various kinds of LEQDs for different applications, adding versatility and flexibility to this technique. Fourth, through lipid enclosure the cytotoxicity of QDs can be minimized, which was proved in a previous study that QDs encapsulated with lipid micelles were not harmful during *Xenopus* development [39]. Fifth, nanoparticle aggregation in cells and *in vivo* can be prevented. Most of the amine-coated nanoparticles are very sensitive to serum; therefore, these nanoparticles tend to aggregate in serum-containing medium or in cytosol. On the contrary, QDs were insulated by GEC-Chol/Chol layers in our case, which prevented them from aggregation even in the presence of serum. As a result, it has the potential to use lipid-coated QDs for measuring optical changes during cell signaling *in vivo*.

#93051 - $15.00 USD Received 22 Feb 2008; revised 26 May 2008; accepted 27 May 2008; published 13 Jun 2008

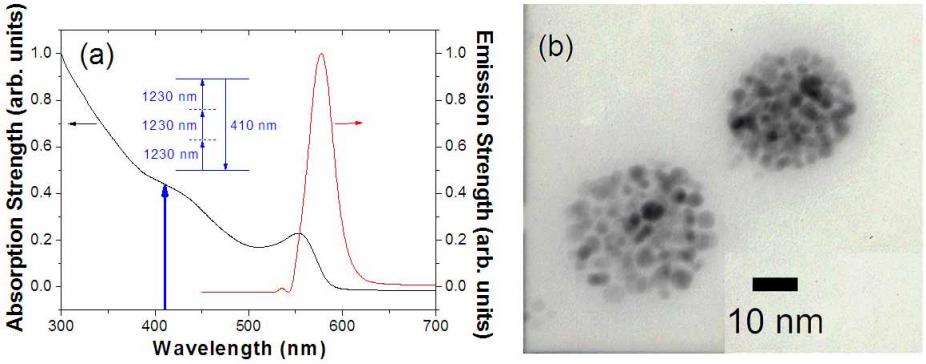

Fig. 1. (a) Absorption and emission spectra of ~5 nm CdSe QDs. Black line: absorption; red line: emission. (b) Transmission electron micrograph of ~100 nm lipid-enclosed CdSe QDs. Scale bar: 10 nm

2.2 Cell cultures

Human cervical cancer cells (HeLa), two human breast cancer cell lines (AU565 and MCF7) and mouse colorectal adenocarcinoma cells (CT-26) were obtained from the American Type Culture Collections (ATCC) (MD, USA). HeLa, MCF7 and AU565 cells were cultured in Dulbecco's Modified Eagle's Medium (DMEM) supplemented with 10% heat-inactivated fetal bovine serum, whereas CT-26 cells were cultured in Roswell Park Memorial Institute (RPMI) medium plus 10% serum. Routine cell culture was carried out at 37 °C with supplementation of 5% CO_2.

2.3 Procedures for loading LEQDs into HeLa and CT-26 cells

HeLa and CT-26 cells (2×10^4-1×10^5) were seeded in each of the 35 mm culture plate wells for 24 hours before loading of LEQDs. Cationic LEQDs of mass 5 μg were incubated with cells in 1.5 ml culture medium at 37 °C for overnight. After brief washing, these cells were either fixed for THG observation or imaged when still living. Due to the cationic surface charge, the loading efficiency of LEQDs to cells was high and therefore the total amount of LEQDs used to load cells was low. In this case nearly all cells (95%) were loaded with LEQDs, which was verified using flow cytometry analysis. Electron microscope pictures also confirmed that cationic lipids help nanoparticles escape from endosomes and stay in the peri-nuclear region.

2.4 Tumor model for THG imaging

Around 5×10^5 of LEQD-loaded CT-26 cells were injected into the dermis tissues of nude mice (Narl: ICR-Foxn1nu) to initiate tumors. After one week, *in vivo* epi-THG images were taken from anesthetized animals. The experimental protocols were approved by the National Taiwan University Institutional Animal Care and Use Committee (NTU-IACUC) and by the National Taiwan University Hospital Institutional Animal Care and Use Committee (NTUH-IACUC).

2.5 Synthesis of anti-Her2 antibody- linked LEQDs

To assemble receptor-targeting LEQDs, protein A-streptavidin (PAST) fusion protein was used as a bifunctional adaptor. The genetically engineered PAST fusion protein was expressed in bacteria, harvested, and then isolated homogeneously by an affinity column. Neutral LEQDs were coated with PAST through biotin linkage. Anti-Her2 antibodies (Herceptin, Genentech Co., CA, USA) were further linked to LEQD surfaces via protein A interaction.

#93051 - $15.00 USD Received 22 Feb 2008; revised 26 May 2008; accepted 27 May 2008; published 13 Jun 2008

2.6 Cell labeling with anti-Her2-linked LEQDs

AU565 and MCF7 cells (2×10^4-1×10^5) were seeded in each of the 35 mm culture plate wells for 24 hours before QD labeling. Anti-Her2-linked LEQDs (1.25 μg) were diluted in 1.5 ml of basal medium, and were subsequently added to each of the culture wells. After incubation for 1 hour, cells were washed with phosphate buffered saline (PBS), replaced with complete medium, and further incubated at 37 °C with the supplementation of 5% CO_2 for another 24 hours before imaging.

2.7 Epi-THG/MPEF microscope

One optical platform with simultaneous epi (reflection) type THG and multiphoton excited fluorescence (MPEF) microscope was developed and adopted in this study [13]. The study of THG microscopy using LEQDs as contrast agents was performed using a home-built femtosecond Cr:forsterite laser centered at 1230 nm with a 130 fs pulsewidth and a 110 MHz repetition rate [8, 15]. The spectral full width at half maximum of the laser output was about 20 nm. The infrared laser beam was first shaped by a telescope, and then directed into a modified beam-scanning system (Olympus FV300) and an upright microscope (Olympus BX51). When the observed cell specimens were placed on glass slides, an infrared (IR) water-immersion objective with a high numerical aperture (NA) and a short working distance (WD) (Olympus UplanApo/IR 60X/ NA 1.2/WD 0.2 mm) was used to increase the spatial resolution and the THG efficiency. For *in vivo* animal studies, an IR water-immersion objective with a 2 mm working distance (Olympus LUMplanFL/IR 60X/NA 0.9/WD 2 mm) was used to perform deep-tissue observation. After anaesthetization, the nude mouse was put under our epi-THG microscope as shown in Fig. 2(b) with an electrical blanket to maintain the body temperature of the test animal. The epi-THG signals were collected using the same objective for illumination; details of the epi-THG microscope can be found in [8]. To ensure the signals we collected were THG, a spectrometer was used to confirm the detected wavelength before imaging and our power-dependent study also verified the cubic dependency of the signals.

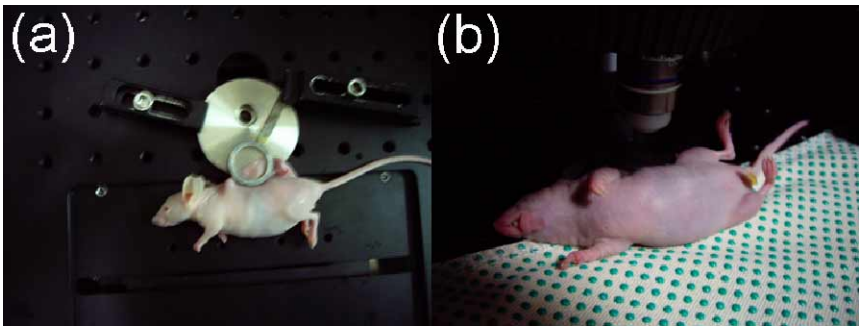

Fig. 2. (a) The tumor region in the dorsal skin was restrained on our home-made device for observation. (b) After anesthetization, the nude mouse was put under our epi-THG microscope with an electric blanket to maintain the body temperature.

2.8 Numerical simulations

Numerical simulations were performed to verify the origin of the detected THG signals. The dyadic Green's function was used to calculate the THG strength both in the epi- and the forward-directions [40]:

$$\mathbf{E}^{(3\omega)}(\mathbf{R}) \propto \iiint_V dV \left(\bar{\mathbf{I}} + \frac{\nabla\nabla}{k_3^2} \right) \frac{\exp(ik_3\mathbf{R}\cdot\mathbf{r})}{|\mathbf{R}|} \cdot \mathbf{P}^{(3\omega)}(\mathbf{r}), \quad (1)$$

#93051 - $15.00 USD Received 22 Feb 2008; revised 26 May 2008; accepted 27 May 2008; published 13 Jun 2008

$$P^{(3\omega)} \propto \int_{\theta} d\theta \int_{0}^{2\pi} d\phi \left| \mathbf{E}^{(3\omega)}(\mathbf{R}) \right|^2 R^2 \sin\theta , \tag{2}$$

where **R** and **r** are coordinates of observation and source points, respectively, $\bar{\mathbf{I}}$ is the idemfactor, ∇ is the dyadic del operator, k_3 is the wave-vector amplitude at 3ω in the matrix, and $\mathbf{P}^{(3\omega)}(\mathbf{r})$ is the laser-induced third-order polarization inside the particle. The value of k_3 is calculated by $k_3 = n_3 \cdot 2\pi / \lambda$, where n_3 = 1.344 is the refractive index of water in this case [41]. To calculate $\mathbf{P}^{(3\omega)}(\mathbf{r})$, the excitation field was modeled as a focused Gaussian beam, and the refractive index of CdSe was calculated with the associated Sellmeier equation [41] to determine the medium-dependent optical distance z inside the particle [42]. The value of 2.523 is used as the refractive index of CdSe at 1230 nm [41]. Because the particle sizes were much smaller than the wavelength, diffraction at the particle-solvent interface was ignored in our calculation. The observation cone angle was defined as θ = 115° to 180° and 0° to 65° for epi-THG and forward-THG (F-THG) calculations, respectively, corresponding to the NA 1.2 objective used in the experiment. The value was calculated by $\alpha = \sin^{-1}(\mathrm{NA}/n_1)$ = 65°, where n_1 is the refractive index at ω in the matrix [40] and is chosen to be 1.325 for water here [41]. The volume of integration V was limited to the particle region assuming that the $\chi^{(3)}$ value of CdSe is much larger than that of the solvent [43]. To take into consideration the polydispersity of particles, the calculated curves were furthermore weighted by a Gaussian-shaped size distribution, with a standard deviation proportional to the particle diameter:

$$P_{poly}^{(3\omega)}(d) \propto \int_{d'} dd' P^{(3\omega)}(d') \cdot \frac{1}{\sigma} \exp\left(-\frac{(d'-d)^2}{2\sigma^2} \right), \tag{3}$$

The standard deviation is calculated by $\sigma = \left(d'/d_{ref}\right) \cdot \sigma_{ref}$, where the referenced standard deviation of size distribution is derived from TEM statistics and is σ_{ref} = 30 nm for d_{ref} = 130 nm.

3. Results and discussion

3.1 Epi-THG characteristics of lipid-enclosed CdSe QDs

There are two strategies to enhance the epi-THG signal from a single nanoparticle. One is to use the resonance effect; the other is to increase its size to the optimum condition, taking advantage of the coherent nature of the THG process. QDs provide the required three-photon resonance effect due to the real transition states at 410 nm, while lipids can help enclose 5 nm QDs into a more suitable size for coherent enhancement. It is interesting to notice that THG from lipids [6] and QDs [32-34] were both reported in previous studies. In our investigations, to determine their relative THG strengths we used the epi-THG microscope to measure different nano-materials in solution, including CdSe QDs, lipid nanoparticles, and LEQDs. In addition to the LEQDs synthesized the same way throughout this paper, whose average diameter was ~130 nm, LEQDs 30 nm in diameter were also prepared for the size dependent study and for further comparisons with the silver nanoparticles we previously reported [27]. The experimental results are shown in Figs. 3(a)-(i). Since the measured epi-THG intensities varied dramatically between these samples, the photomultiplier tube (PMT) was supplied with different voltages ranging from 800 to 1200 V. To analyze these data, each THG image could be regarded as an array of 512×512 individual measurements. During the integration time at each pixel, particles showed up stochastically inside the confocal volume and were sampled at the repetition rate of the excitation laser. THG intensity signals from different laser pulses were then added as the final pixel intensity recorded by the computer. As a result, the average epi-THG power of one single particle can be calculated by first averaging the pixel intensities of all frames in each THG image and then weighted with different PMT voltages. Finally, relative particle concentrations between samples were also taken into consideration, because a

#93051 - $15.00 USD Received 22 Feb 2008; revised 26 May 2008; accepted 27 May 2008; published 13 Jun 2008

fixed amount of lipids was used to synthesize each specimen and the concentration would be a function of the particle size. The mathematical equation is expressed as

$$I(d) \propto \left[\frac{1}{f} \sum_f \left(\frac{1}{512 \times 512} \sum_{m=1}^{512} \sum_{n=1}^{512} S(f,m,n) \right) \right] \cdot y(V) \cdot d^3, \quad (4)$$

where *f* is the number of frames in the image, *S(f,m,n)* is the pixel intensities of the image, *y(V)* is the experimentally-determined weighting factor of the PMT output as a function of the supplied voltage *V*, and *d* is the measured particle size. The simulation results were then fitted to the experimental data by

$$I(d) \approx C \cdot P_{poly}^{(3\omega)}(d), \quad (5)$$

where *C* is a fitting constant accounting for the effective $\chi^{(3)}$ inside LEQDs, all reflection/absorption losses of signals, and all constant terms dropped in Eqs. (1)-(4) to speed up calculation. Since a common value of *C* is used to fit all data of different LEQD diameters, the fitting process was performed to address the size dependence instead of the resonance effect. The measured relative epi-THG intensity of one single LEQD, lipid nanoparticle (GEC-Chol/Chol, 1:1) and CdSe QD is then plotted in Fig. 3(j) as a function of particle diameter, along with the simulation results on direct-epi- and forward-THG from LEQDs, with *C* as the only fitting constant. Using the sampling model aforementioned, numerical simulations were performed by positioning the particle at different locations inside the confocal volume, and the calculated THG intensities were then added. The calculated curve in this way deviated by less than 5% from the curve assuming a fixed particle at the center of the focus when normalized to the same scale, so the latter fixed-position approach could also be used to expedite the calculation. Due to the coherent THG process, when the particle size is much smaller than the THG wavelength, the generated THG field intensities from different parts of the nanoparticle constructively interfere with each other, causing the $\propto d^6$ power increase with the particle size for both forward and backward THG [44], as has been reflected by the simulation curves shown in Fig. 3(j). However, when the particle size increases to a fraction of the THG wavelength (100 nm in our case), the epi-collected THG field intensities generated from different parts of the nanoparticle will start to show phase variations, due to different excitation time and due to different distances from the detector, thus starting to cause destructive interference. This coherent saturation effect limits the optimized particle size for epi-THG detection, which is slightly larger than $\Delta x \approx \hbar / \Delta p$ due to the 3D shape of the nanoparticle, where Δp is the momentum mismatch between three incoming 1230 nm photons and one epi-detected THG photon.

In addition to the curves assuming monodisperse LEQDs, which are shown as cyan and dark yellow dashed lines in the figure, curves assuming a Gaussian-shaped particle-size distribution are also plotted as solid lines. As can be seen in the figure, the experimental data fit very well to the simulation on direct-epi-THG with polydispersity (black solid line) but deviate obviously from the trace of the forward-THG (red solid line), supporting the proposed coherent saturation effect. With a 1230 nm excitation light, the optimized nanoparticle size for epi-THG detection is thus around 100 nm. In the following reported imaging experiments, we used LEQDs 130 nm in diameter for efficient THG generation. This size-dependent experiment also suggested that the signals we measured were direct-epi-THG, not forward-THG back-scattered after generation.

#93051 - $15.00 USD Received 22 Feb 2008; revised 26 May 2008; accepted 27 May 2008; published 13 Jun 2008

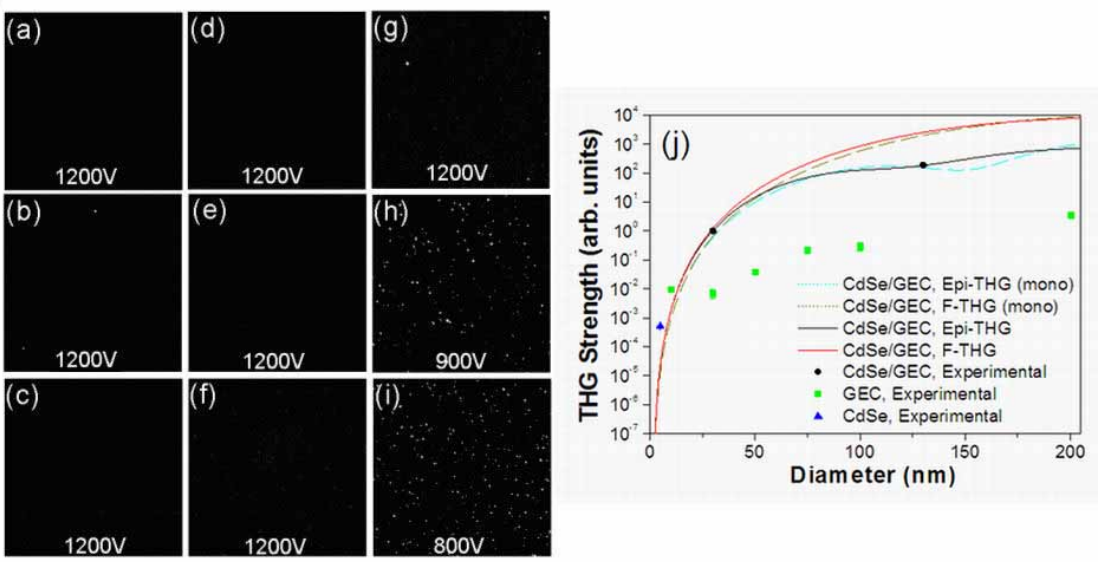

Fig. 3. Epi-THG intensities of nanoparticles with different sizes and materials. Figures (a)-(i) show the epi-THG images with different materials in solution: (a) Deionized water; (b) 10 nm GEC lipid nanoparticles; (c) 50 nm GEC lipid nanoparticles; (d) 100 nm GEC lipid nanoparticles; (e) 200 nm GEC lipid nanoparticles; (f) 100 nm DPPC lipid nanoparticles; (g) 5 nm CdSe QDs; (h) 30 nm GEC-lipid-enclosed CdSe QDs; (i) 130 nm GEC-lipid-enclosed CdSe QDs; (j) Epi-THG power vs. diameter for GEC-lipid-enclosed CdSe QDs (black circle), GEC lipid nanoparticles (green square), and ~5 nm CdSe QDs (blue triangle). Cyan and dark yellow dashed lines represent epi-THG and F-THG, respectively, from monodisperse LEQDs; black and red lines represent epi-THG and F-THG, respectively, assuming a Gaussian distribution in polydispersity. Epi-THG intensities from CdSe QDs and GEC lipid nanoparticles are much weaker than those from GEC-lipid-enclosed CdSe QDs.

The influence of the multiple-interface effect inside LEQDs is discussed here. The particles used in our experiments had a maximum diameter of ~130 nm, which is much smaller than the excitation wavelength of 1230 nm. Since each LEQD contained more than tens of 5 nm CdSe quantum dots, the spacing between QDs inside the sphere would be on the order of 10 nm or less. As a result, the multiple-interface effect should not be a dominant factor in the observed strong THG from LEQDs, because such an effect is the result of the Gouy phase shift effect and is obvious only when interfaces are separated by a distance comparable to the confocal parameter. Inside our LEQDs, THG field intensities generated from these closely-packed QDs would have a coherent phase relationship determined by their separation distance, rather than experiencing different phase shifts due to the Gouy effect, which is the cause of the usually called interface effect. To verify this concept, we performed additional simulations for verification. The sample structure used in the simulation consisted of two thin slabs 10 nm in thickness, separated by a distance ranging from 0 to 100 nm, as shown in Fig. 4(a). The $\chi^{(3)}$ value of the surrounding matrix was assumed to be much smaller than that of the slab, so THG from the matrix was ignored. The focal position of the incident Gaussian beam was scanned across the entire sample structure, and the maximum value in each scan was recorded. Because of the nature of this layered structure, a phase correction term has to be added to the excitation beam in the second slab region, which can be derived as

$$\Delta\phi = -\frac{2\pi}{\lambda}\left(\frac{n_{1,slab}^2}{n_{1,medium}} - n_{1,medium}\right)\cdot\delta, \qquad (6)$$

where δ is the separation distance between two slabs. The wavelength was set to 1230 nm, NA to 1.2, cone angle to 65°, and material parameters of CdSe and water were used for the

#93051 - $15.00 USD Received 22 Feb 2008; revised 26 May 2008; accepted 27 May 2008; published 13 Jun 2008

slab and the medium regions, respectively, as described in Section 2.8. The result is plotted in Fig. 4(b). As can be seen from the figure, when the slab thickness and spacing between them are much smaller than the wavelength, increasing the total number of interfaces does not necessarily lead to stronger THG signals. It is the total volume and the coherent effect that determined the measured THG intensity. This is especially obvious in epi-THG, because destructive interference can cause significant signal reduction at specific intervals of slab separation.

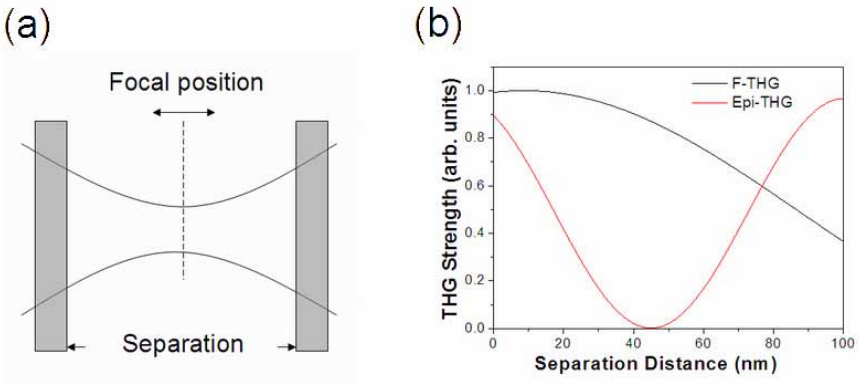

Fig. 4. (a) Schematic of the structure used in simulations to illustrate the coherent versus the multiple-interface effects. The thickness of each slab is 10 nm, while the separation between them is 0-100 nm. (b) Simulation results on the intensities of forward- and epi-THG from the structure. Black line: forward-THG; red line: epi-THG.

Our study also supports the design of three-photon resonance of THG. Previous studies have shown that THG can be enhanced when the virtual-state process matches a real electron transition in materials [19, 20, 45]. Referring to Fig. 1, the LEQDs we synthesized contained an aggregation of 5 nm CdSe QDs, corresponding to an emission wavelength of 580 nm [46]. Since the absorption of quantum dots strongly increases for wavelengths shorter than their emission wavelength [46], including the THG wavelength of 410 nm in this case, lots of real transition states can be found in this spectral region to match the THG process. In comparison, as shown in the experimental results, the epi-THG intensities from lipid nanoparticles without QDs were several orders weaker even for diameters up to 100 nm. It should also be noted that the 30 nm LEQDs even outperformed the plasmon-resonance-enhanced 30 nm silver nanoparticles previously reported [27] by a factor of 20X. It is such brightness that makes the LEQDs competent contrast agents in epi-THG microscopy.

3.2 Imaging LEQDs in cells using epi-THG microscopy vs. MPEF microscopy

QDs are efficient fluorophores for confocal and MPEF microscopy techniques. They can thus provide fluorescence signals to reflect the degree of absorption due to the effect of three-photon-resonance enhancement, which causes THG contrast agents to absorb the excitation light through three-photon absorption or through generated third-harmonic waves [45]. To quantitatively compare signal intensities of THG and fluorescence from LEQDs, HeLa cells were loaded with LEQDs and then imaged with our microscope, which simultaneously recorded THG and MPEF images. As mentioned in Section 2.1, one advantage of using LEQDs is that we can choose different lipids to synthesize various kinds of LEQDs for different applications, adding versatility and flexibility to this technique. As a result, the composition of cationic cholesterol (GEC-Chol) and standard cholesterol in a 1:1 molar ratio was used to facilitate cell uptake because cationic LEQDs could be efficiently absorbed by cells due to additional positive charge on their surfaces. Figure 5(a) shows one measured epi-direction spectrum of the LEQDs excited by our fs Cr:forsterite laser. Strong epi-THG signals, > 20 times larger than the three-photon fluorescence (3PF) signals around 580 nm, could be

#93051 - $15.00 USD Received 22 Feb 2008; revised 26 May 2008; accepted 27 May 2008; published 13 Jun 2008

detected and there was no crosstalk between THG and 3PF. This result is twofold in significance. From one point of view, our measurement verified that with the same signal intensities, the light absorption in contrast agents due to the effect of real-state-resonance enhancement in epi-THG microscopy is > 20X less than the corresponding fluorescence-based technologies. From the other, with the same amount of energy deposition into contrast agents, epi-THG in LEQDs can provide much brighter signals over fluorescence-based modalities, not to mention the adopted laser can also offer much reduced energy deposition into surrounding biotissues. Compared with the fluorescence microscopy using quantum dots, THG microscopy using LEQDs can therefore simultaneously yield a better signal-to-noise ratio (SNR) and result in much reduced photodamage. Furthermore, unlike fluorescence from QDs, no photoblinking or photobleaching was observed when these LEQDs were imaged using epi-THG microscopy, which provides another advantage of this virtual-transition-based technique. To visually verify this result, Fig. 5(b) shows a typical epi-THG image of LEQD-loaded HeLa cells, in which bright spots can be clearly seen in the cytosol region. Figure 5(c) shows the simultaneously acquired 3PF image after normalization, with the 3PF wavelength corresponding to the QD fluorescence wavelength. Because the THG intensities were much stronger than 3PF, Fig. 5(b) contained most of the bright spots in (c) and revealed more information than fluorescence. Under the experimental condition with a low PMT voltage, the possibility was excluded that these extra spots were from intrinsic cell structures. The result in Fig. 5(b) is then significant in several ways for LEQDs to be eligible contrast agents for epi-THG microscopy *in vivo*. First, the epi-THG signals were strong in Fig. 5(b), indicating that LEQDs were efficient epi-THG generators in cells. Second, because the HeLa cells were washed before imaging (see Section 2.3), dead cells and particles suspending in solution would be carried away by the procedure; for THG to be observed from LEQDs, these particles must be able to penetrate into cells on one hand and have no immediate toxicity on the other. For further verification, those cells were cultured for additional 48 hours after washing and their viability was confirmed using MTT assay. From the experimental results, it can be concluded that these LEQDs can be effectively absorbed by cells, pose no immediate toxicity to them, and can be efficiently observed through epi-THG. These features are critical in choosing contrasts agents for microscopy *in vivo*, and the LEQDs we developed clearly meet these criteria and are suitable for applications like cell tracking.

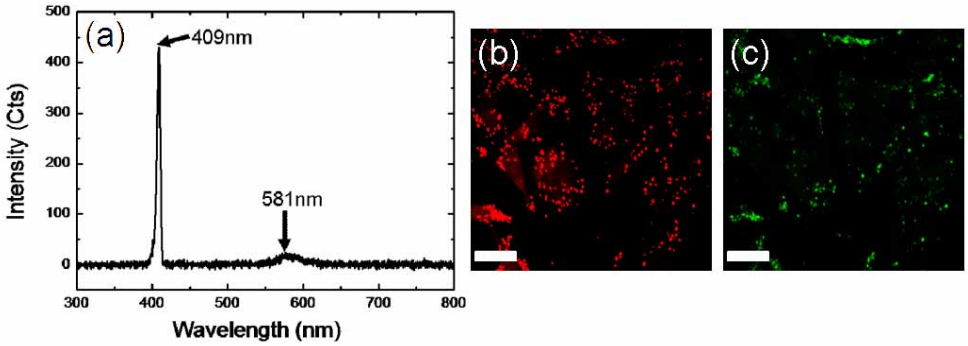

Fig. 5. One typical measured backward emission spectrum of these LEQDs excited by our fs Cr:fosterite laser is shown as (a). The observed epi-THG was ~20X stronger than the 3PF from the LEQDs. The cationic LEQDs in HeLa cells were also imaged by (b) THG microscopy and (c) 3PF microscopy. Scale bar: 20 μm.

3.3 In vivo *tumor cell tracking by epi-THG microscopy*

Having demonstrated that LEQDs can be inserted into cells as bright epi-THG contrast agents, a study was performed to show their ability to assist cell tracking in live animals. We chose

#93051 - $15.00 USD Received 22 Feb 2008; revised 26 May 2008; accepted 27 May 2008; published 13 Jun 2008

nude mice as an animal model and conducted experiments *in vivo*. First, we prepared cationic LEQDs (GEC-Chol/Chol 1:1) as described in Section 2.1 since they can be effectively absorbed by cells. These LEQDs then escaped from endosomes and stayed in the peri-nuclear region of these loaded cells. More than 95% of the cultured cells could be loaded with LEQD efficiently, which was verified using flow cytometry analysis. Furthermore, long-term cell viability was also larger than 85%, analyzed using MTT assay. We then injected the LEQD-loaded CT-26 cells into the dermis tissues of nude mice to induce mouse colonic tumor. After one week, the initially injected tumor cells grew to a size of 0.5-1 cm, indicating that they did not suffer necrosis from LEQDs and were able to multiply and proliferate. The epi-THG microscope was used to image the tumor region *in vivo* as shown in Fig. 2. As a control experiment we also imaged three nude mice *in vivo*, over five different normal regions each. By adjusting the imaging system to a relatively low sensitivity level with a low PMT voltage of 1000 V (compared with high sensitivity of 1200 V), in most cases, we could not observe significant THG from cells at a depth greater than ~100 μm in the subcutaneous tissues, as shown in Fig. 6(a). On the other hand, with the same low sensitivity level, Fig. 6(b) shows the images of tumor cells loaded with LEQDs, in which significant THG could be observed at a depth over 100 μm in the subcutaneous tissues and the signals were at least 20X stronger compared with the previous figure. In Fig. 6(b) endogenous cell structures like membranes were no longer clearly seen in the tumor region because signals from them were overshadowed by strong THG intensities from LEQDs. Uniform epi-THG intensities can be seen, indicating high labeling uniformity in cancer cells. This proves again the point of our study that THG contrast can be manipulated, and to our knowledge this is the first time that THG contrast can be manipulated *in vivo* using nanopatciles in a living animal deep inside skin tissues. It should also be noted that after one week the LEQDs were still lodged in the tumor region, unaffected by either catabolism or metabolism. After imaging, we further analyzed tumor xenograph through biopsy, which revealed that most of the LEQDs were located in tumor cells. Very few macrophages had infiltrated into the tumor part at the early stage of tumor formation. These results illustrate again that our LEQDs are stable in living cells and are potentially biocompatible. Stable in biochemical environments and bright in THG emission, the LEQDs prove to be powerful contrast agents in cell tracking, such as in our study of the distribution of cancer cells in nude mice. Combining these LEQDs with a 1230 nm laser, our THG modality thus provides 3D *in vivo* observation with minimum invasion and high spatial resolution. Other possible applications may include the tracing of stem cells or tumor proliferation *in vivo* in the future because long-term observation is required under these circumstances.

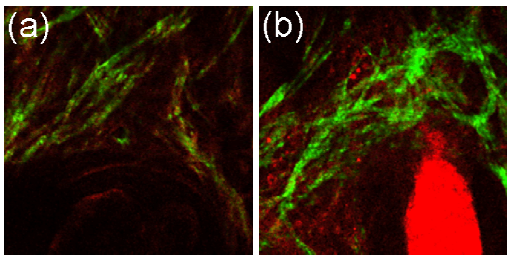

Fig. 6. (a) (539 kB) An example movie shows a stack of depth-resolved *in vivo* horizontal sections from epi-harmonic generation microscopy in normal subcutaneous tissues of a nude mouse. Depth range: 70-100 μm. (b) (1.76 MB) An example movie shows a stack of depth-resolved *in vivo* horizontal sections in the subcutaneous tissues in the tumor-induced region loaded with LEQD. The red color represents epi-THG and the green epi-SHG. Depth range: 70-120 μm. Image size: 120×120 μm.

#93051 - $15.00 USD Received 22 Feb 2008; revised 26 May 2008; accepted 27 May 2008; published 13 Jun 2008

3.4 Epi-THG Detection of Her2 Expression in live breast cancer cells

In the previous section we illustrated the function of LEQDs in their intrinsic form, but their capabilities can be further extended by suitable modification. As a demonstration, we chose cultured human breast cancer cells to evaluate their ability to target specific molecular expression in live cells. Specifically, the Her2 oncogene encodes a transmembrane receptor for epidermal growth factors and plays a key role in cell growth and anti-apoptotic signaling [47-49]. It is known to be very important in cancer development, clinical prognosis, and therapeutic applications [50-52]. Overexpression of Her2/neu in cancer lesion is an index of unfavorable clinical outcome, with more aggressive growth behavior and resistance to some chemotherapy agents [51, 52]. One particular type of antibodies, the therapeutic antibody Herceptin, binds to Her2 and enhances apoptosis of these aggressive tumor cells [53], and we combined these antibodies with our LEQDs to monitor Her2 receptors in living cells. In this case, efficient cell uptake should be avoided to discriminate between different cell lines, so neutral lipids (DPPC) were used to synthesize the LEQDs. These antibody-linked LEQDs were further incubated with AU565 (overexpression of Her2/neu receptors) and MCF7 (low-level expression of Her2/neu receptors) breast cancer cells, respectively. The acquired epi-THG images are shown in Fig. 7. In the epi-THG images of cells not incubated with LEQDs, Figs. 7(b) and (e), only weak signals could be detected from cell membranes and organelles when the contrast was tune down to the same level as other images. In the images of cells incubated with standard neutral LEQDs, only a few bright spots could be observed. Comparing Fig. 5(b) with Figs. 7(c) and (f), our results indicate that it is difficult for neutral LEQDs to penetrate into cells, which justified our choice. So far the two sets of images on different cell lines do not differ significantly, but the distinction becomes apparent for images with antibody-linked LEQDs. In Fig. 7(d), abundant bright THG spots could be clearly observed in AU565 cancer cells. It is also interesting to notice that the cells in Fig. 7(d) were relatively uniformly-labeled and the standard deviation of epi-THG signal intensities per cell was ~25% of the average value. Compared with the much reduced THG spots observed in MCF7 cancer cells in Fig. 7(g), our result agreed well with these cell lines' respective endogenous Her2 expression levels, since AU565 cells are 100X stronger than MCF7 cells in expression [54]. As a result, our antibody-linked LEQDs successfully detected specific molecular expression and discriminated between different cell lines.

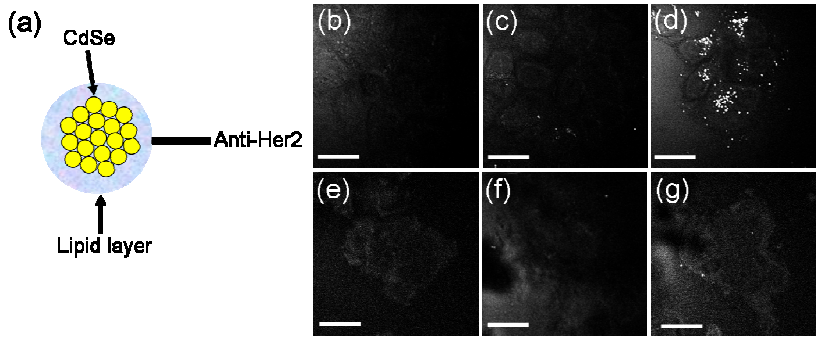

Fig. 7. Demonstration of THG imaging using anti-Her2-linked neutral LEQDs as contrast agents to identify the Her2 expression in live breast cancer cells with normal (MCF7) and high (AU565) expression. (a) Schematic of anti-Her2-linked LEQDs (b) THG image of AU565 cells not applied with LEQDs. (c) THG image of AU565 cells applied with LEQDs. (d) THG image of AU565 cells applied with anti-Her2-linked LEQDs. (e) THG image of MCF7 cells not applied with LEQDs. (f) THG image of MCF7 cells applied with LEQDs. (f) THG image of MCF7 cells applied with anti-Her2-linked LEQDs. Scale bar: 30 μm. Rich bright THG spots can only be observed in the AU565 cells applied with anti-Her2-linked LEQDs, and thus our developed THG microscopy can identify the Her2 expression levels in live breast cancer cells with normal and overexpressing Her2 receptors.

#93051 - $15.00 USD Received 22 Feb 2008; revised 26 May 2008; accepted 27 May 2008; published 13 Jun 2008

4. Conclusion

In this paper, we developed lipid-enclosed CdSe quantum dots as a new type of contrast agents in THG microscopy. They are efficient THG generators, 20X brighter than the silver nanoparticles we previously reported. They are potentially more biocompatible than pure quantum dots and possess no immediate biohazard in nude mice and cultured human cells. By injection of LEQD-loaded cancer cells into nude mice, the tumor region could be clearly imaged with epi-THG microscopy *in vivo* after one week, even deep in subcutaneous tissues. By linking LEQDs with anti-Her2 antibodies, the expression levels of Her2/neu receptors in two live cell lines of human breast cancer could be imaged and distinguished by our epi-THG microscope.

Compared with fluorescence microscopy using quantum dots, as THG contrast agents these LEQDs have no photobleaching or photoblinking problems, which allows long-term tracing of cell positions or molecular expression. In addition, even with an epi-collection scheme our developed LEQDs can generate THG signals 20X stronger than fluorescence, thus achieving a higher SNR and better penetration capability when the energy deposited in quantum dots are kept the same. If fluorescence signals are to reach the same intensities as THG, then more energy has to be stored in quantum dots for more fluorescence relaxation. Compared with the 1230 nm laser used in our experiments, in confocal or two-photon fluorescence microscopy a shorter wavelength is typically used for excitation, which reduces the penetration depth and may bring more photodamage to biological specimens. Combining a 1230 nm laser and the LEQDs we demonstrated, deeper penetration and higher cell survivability can be achieved, which in turn enables long-time observation on a grander time scale. Bright, biocompatible and versatile, the developed LEQDs prove to be a competent type of contrast agents in THG microscopy *in vivo*. Our study suggests that these LEQDs can be used in various types of biological applications in the future.

Acknowledgments

The authors gratefully acknowledge financial support from the National Health Research Institute (NHRI-EX97-9201EI), National Science Council (NSC96-2120-M-002-014; NSC96-2320-B-002-086), National Taiwan University Research Center for Medical Excellence-Division of Genomic Medicine, and Frontier Research of National Taiwan University.

#93051 - $15.00 USD Received 22 Feb 2008; revised 26 May 2008; accepted 27 May 2008; published 13 Jun 2008